

On the efficiency of jet production in FR II radio galaxies and quasars

Katarzyna Rusinek^{1,2*}, Marek Sikora^{2†}, Dorota Koziel-Wierzbowska³,
Leith Godfrey⁴

¹*Toruń Centre for Astronomy, Faculty of Physics, Astronomy and Informatics, Nicolaus Copernicus University, Grudziądzka 5, 87-100 Toruń, Poland*

²*Nicolaus Copernicus Astronomical Center, Polish Academy of Sciences, Bartycka 18, 00-716 Warsaw, Poland*

³*Astronomical Observatory, Jagiellonian University, ul. Orla, 30-244 Kraków, Poland*

⁴*ASTRON, the Netherlands Institute for Radio Astronomy, Postbus 2, 7990 AA, Dwingeloo, The Netherlands*

21 December 2016

ABSTRACT

Jet powers in many radio galaxies with extended radio structures appear to exceed their associated accretion luminosities. In systems with very low accretion rates, this is likely due to the very low accretion luminosities resulting from radiatively inefficient accretion flows. In systems with high accretion rates, the accretion flows are expected to be radiatively efficient, and the production of such powerful jets may require an accretion scenario which involves magnetically arrested discs (MADs). However, numerical simulations of the MAD scenario indicate that jet production efficiency is large only for geometrically thick accretion flows and scales roughly with $(H/R)^2$, where H is the disc height and R is the distance from the BH. Using samples of FR II radio galaxies and quasars accreting at moderate accretion rates we show that their jets are much more powerful than predicted by the MAD scenario. We discuss possible origins of this discrepancy, suggesting that it can be related to approximations adopted in MHD simulations to treat optically thick accretion flow within the MAD-zone, or may indicate that accretion disks are geometrically thicker than the standard theory predicts.

Key words: quasars: jets – radiation mechanisms: non-thermal – acceleration of particles

1 INTRODUCTION

The radio-loudness of a quasar is defined as the ratio of radio luminosity (typically at 5 GHz) to optical luminosity (typically in the B-band). The radio luminosity of a quasar is related to jet power P_j , while the optical luminosity is related to accretion power $\dot{M}c^2$, where \dot{M} is the accretion rate. For this reason, the radio-loudness is a proxy for the jet production efficiency defined to be $\eta_j \equiv P_j/(\dot{M}c^2)$.

The first quasars were discovered following the identification of bright radio sources with point-like optical sources. However, not all quasars have such strong radio emission: in fact, the majority of quasars have been found to be radio-quiet (Kellermann et al. 1989). Present-day radio telescopes are able to detect the faint radio emission of radio-quiet quasars (e.g. White et al. 2015, and refs. therein), however, their radio loudness is up to 3–4 orders of magnitude lower

than that of the radio loudest AGNs (e.g. White et al. 2007). This indicates a large diversity of jet production efficiency.

There have been several scenarios proposed to explain such a diversity of jet production efficiency. The two most popular scenarios are the so-called “spin paradigm” (Wilson & Colbert 1995; Sikora et al. 2007; Garofalo et al. 2010; Fanidakis et al. 2011) and the intermittency of jet production (Livio et al. 2003; Körtling et al. 2006). According to the spin paradigm the jets are powered by rotating BHs and the jet production efficiency, η_j , is assumed to depend predominantly on the value of the BH spin. The drawback of this assumption is that it implies much lower values of BH spin in radio-quiet AGN than indicated by using “Softan argument” (Soltan 1982; Elvis et al. 2002; Lacy et al. 2015) and predicted by numerical simulations of cosmological evolution of supermassive BHs (Volonteri et al. 2013). The intermittent jet production scenario involves transitions between two accretion modes: one associated with a standard viscous accretion discs and another associated with accretion being driven by MHD winds. While this scenario may be attractive to explain intermittent jet activity observed directly in

* E-mail: krusinek@camk.edu.pl (KR)

† E-mail: sikora@camk.edu.pl (MS)

GRS 1915+105 (Livio et al. 2003) and the overabundance of compact radio galaxies in flux limited samples (Reynolds & Begelman 1997), such accretion mode transitions are rather difficult to reconcile with the existence of $10^7 - 10^8$ years old jets observed in FR II radio sources (Blundell et al. 1999; Bird et al. 2008; O’Dea et al. 2009; Antognini et al. 2012) and also with the lack of evidence for remnant radio lobes around radio-quiet quasars (Godfrey et al., in prep). Furthermore, the “transition” models predict bimodal distribution of radio-loudness (e.g. Nipoti et al. 2005) and this is observed only if ignoring other than FR II sources (Lu et al. 2007; Rafter et al. 2011).

Jet production theories are challenged not only by the large spread of radio-loudness, but also by the fact that the jet powers in many radio galaxies reach values comparable to the accretion powers (Rawlings & Saunders 1991; Punsly 2007; Fernandes et al. 2011; Sikora et al. 2013). In order to produce jets with such high efficiency in the Blandford-Znajek mechanism (Blandford & Znajek 1977), BHs are required not only to be spinning very fast but also to be threaded by a very large magnetic flux. The required level of magnetic flux threading the black hole can only be maintained if it is confined by the ram pressure of the accretion flow. The latter condition implies a magnetically arrested disc (MAD) scenario, in which the innermost portion of the accretion flow is dynamically dominated by the poloidal magnetic field and accretion proceeds via interchange instabilities (Narayan et al. 2003; Igumenshchev 2008; Punsly et al. 2009; Tchekhovskoy et al. 2011; McKinney et al. 2012).

Recent studies of the jet powers in a sample of radio selected FR II quasars by van Velzen & Falcke (2013) (see also van Velzen et al. 2015) show that the median jet production efficiency in these objects is tens times lower than maximal predicted by the MAD scenario. Such low jet production efficiency in the MAD scenario would require very low median BH spin and this led the authors to conclude that jet production in these systems does not involve magnetically arrested discs. However, the MAD models predict that the jet production efficiency depends not only on the BH spin, but also has a very strong dependence on the geometrical thickness of the accretion flow. According to Avara et al. (2016) the jet production efficiency at moderate accretion rates, where standard theory predicts very thin accretion discs, should be hundreds of times lower than that obtained from geometrically thick accretion discs. Therefore, due to the strong dependence of jet production efficiency on disc thickness, the problem is actually the opposite of the one claimed by van Velzen & Falcke, and can be expressed by the following question: how is it possible to obtain such high jet production efficiency in these radio-loud AGN, despite their apparently moderate accretion rates, and therefore geometrically thin accretion discs.

In the current work, we demonstrate the presence of high- η_j objects at moderate accretion rates, by considering the dependence of P_j/L_d on the Eddington ratio L_d/L_{Edd} (where L_d is the accretion luminosity and L_{Edd} is the Eddington luminosity) for the following radio-loud AGN samples: $z < 0.4$ FR II NLRGs (Sikora et al. 2013) in §2.2; FR II quasars (van Velzen & Falcke 2013) in §2.3; $0.9 < z < 1.1$ NLRGs (Fernandes et al. 2011) in §2.4; and a sample of BLRG+RLQ (Broad-Line Radio Galaxies plus Radio-Loud Quasars) compiled by Sikora et al. (2007) in §2.5. The the-

oretical implications of the presented distributions – with particular reference to the applicability of the MAD scenario – are discussed in §3 and summarized in §4.

We have adopted the Λ cold dark matter cosmology, with $H_0 = 70 \text{ km s}^{-1}$, $\Omega_m = 0.3$ and $\Omega_\Lambda = 0.7$.

2 JET PRODUCTION EFFICIENCY

2.1 Overview

In order to adequately assess the distribution of radio galaxies and quasars in the $P_j/L_d - L_d/L_{\text{Edd}}$ plane, we have combined four different samples of radio galaxies and quasars. In the following, we describe each of these samples, and the methods used to estimate P_j , L_d , and L_{Edd} from the available radio and optical data.

2.2 FR II NLRGs at $z < 0.4$

This sample contains 207 FR II narrow-line radio galaxies extracted from the sample of $z < 0.4$ radio galaxies with extended radio structure selected by Sikora et al. (2013). The objects are taken from Cambridge catalogs and matched with the SDSS, FIRST and NVSS catalogs. The sample is presented in Table A1 (Appendix A, as subsequent tables), where additionally to data presented in Sikora et al. we list values of: disc luminosities – L_d ; jet powers – P_j ; their ratio – P_j/L_d ; and the Eddington ratio – $\lambda_{\text{Edd}} \equiv L_d/L_{\text{Edd}}$. The disc luminosities L_d are calculated using the $\text{H}\alpha$ emission line luminosity, $L_{\text{H}\alpha}$, which is available for 152 sources, adopting the conversion formula

$$L_d[\text{erg s}^{-1}] = 7.8 \times 10^{36} L_{\text{H}\alpha}[\text{L}_\odot] \quad (1)$$

(Netzer 2009), which gives the disc luminosity with uncertainty 0.3 dex. The jet powers are calculated using the 1.4 GHz monochromatic radio luminosity, $L_{1.4}$, along with the scaling relation of Willott et al. (1999)

$$P_j[\text{erg s}^{-1}] = 5.0 \times 10^{22} (f/10)^{3/2} (L_{1.4}[\text{W Hz}^{-1}])^{6/7}, \quad (2)$$

where we have assumed the radio spectral index between 151 MHz and 1.4 GHz is $\alpha_r = 0.8$ (using the convention $F_\nu \propto \nu^{-\alpha}$). The formula is based on calorimetry of radio lobes and f is the parameter accounting for errors in the model assumptions. According to Blundell & Rawlings (2000) the value of f is between 10 and 20. More secure determination of jet power in FR II radio sources is based on the model of hotspots (Godfrey & Shabala 2013). Unfortunately hotspots are often very weak or not visible. However, comparing jet powers of luminous FR II sources obtained using the hotspots and radio lobe calorimetry allowed us to calibrate the Willott et al. formula. For luminous FR II sources this gives $f \simeq 10$ and uncertainty of P_j calculated using Equation 2 is about 0.3 dex.

The distribution of P_j/L_d for this sample is plotted in Fig. 1. For many objects $P_j/L_d > 10$, which for disc radiation efficiency $\epsilon_d \equiv L_d/(\dot{M}c^2) = 0.1$ implies jet production efficiency $\eta_j \equiv \epsilon_d(P_j/L_d) > 1$, where \dot{M} is the accretion rate.

In Fig. 2 we plot the ratio P_j/L_d against the Eddington scaled accretion luminosity, or Eddington ratio, $\lambda_{\text{Edd}} \equiv L_d/L_{\text{Edd}}$. As can be seen in this figure, the extreme

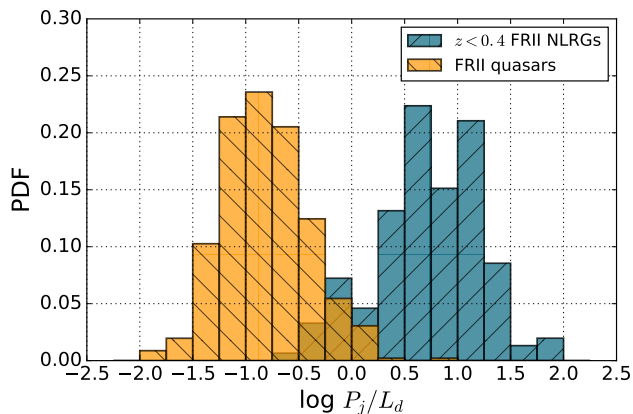


Figure 1. The distribution of the jet efficiency P_j/L_d for $z < 0.4$ FR II NLRGs (152 sources) and FR II quasars (458 sources) samples represented by blue and orange color respectively. The histogram has been normalised so that the sum of the bin heights is equal to unity.

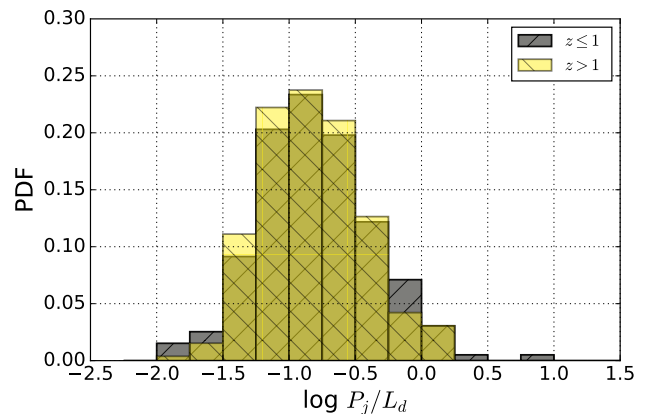


Figure 3. The division of FR II quasars sample (458 sources as it is in Fig. 1) based on the boundary value of redshift $z = 1$. No discrepancy between sources with lower (197 objects marked by grey color) and higher (261 objects represented by yellow color) values is present.

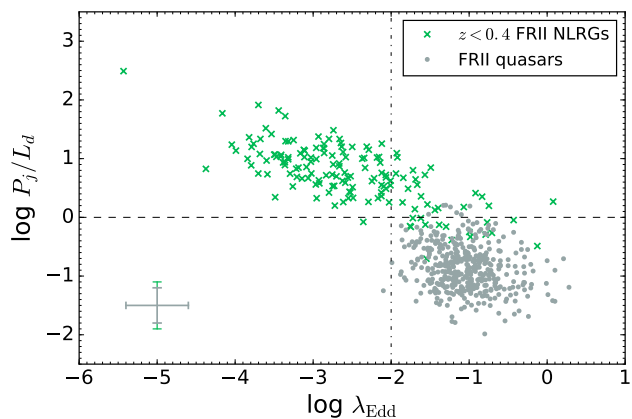


Figure 2. The dependence of P_j/L_d ratio on the Eddington ratio λ_{Edd} . The $z < 0.4$ FR II NLRGs sample is shown by green crosses while grey dots are for FR II quasars sample (here 414 sources). Uncertainties of P_j/L_d and λ_{Edd} (described in the respective subsections) are presented in the lower left corner. The horizontal dashed line corresponds to the level where P_j equals L_d and the vertical dot-dashed line marks an approximate value of the Eddington ratio at which the accretion mode is changing from the radiatively inefficient (left side) to the radiatively efficient (right side) (Best & Heckman 2012; Mingo et al. 2014). An apparent anti-correlation exists between these two plotted properties.

efficiencies with $P_j/L_d > 10$ and hence $\eta_j > 1$ are possessed only by radio galaxies with very low Eddington ratios, which are therefore presumably operating in the radiatively inefficient accretion regime. The median value of P_j/L_d at moderate accretion rates corresponding to $\lambda_{\text{Edd}} > 0.003$ is 2.65, implying a modest jet production efficiency of order $\eta_j \sim 0.265(\epsilon_d/0.1)$. Marked in the lower left corner of Fig. 2 are the uncertainties for P_j/L_d and λ_{Edd} . These are calculated based on the uncertainties for P_j , L_d and M_{BH} and noting that standard deviations of ratios (and products) of two independently determined quantities, $\sigma_{X/Y} = \sqrt{\sigma_X^2 + \sigma_Y^2}$.

The uncertainties of P_j , L_D and M_{BH} are estimated to be approximately 0.3 dex (for the latter see Tremaine et al. 2002), resulting in 0.4 dex uncertainties of P_j/L_d and of $\lambda_{\text{Edd}} \propto L_d/M_{\text{BH}}$.

2.3 The FR II quasar sample

The FR II quasar sample used in this work was first obtained by van Velzen et al. (2015) based on the selection of double-lobed radio sources from the FIRST survey catalog, and cross-matching with SDSS quasars. In Table A2 we present the relevant data for this sample, including the monochromatic rest-frame luminosity at 1.4 GHz, $L_{1.4}$, and if available, masses of black holes and Eddington ratios. The radio luminosities were calculated based on the 1.4 GHz lobe flux densities given by van Velzen et al., and k-corrected assuming radio spectral index $\alpha_r = 0.85$, along with standard Λ CDM cosmology, as specified in Section 1. The jet power P_j was calculated using Equation 2. The black hole masses and Eddington ratios, when available, were taken from Shen et al. (2011) thereby reducing the sample from 458 to 414 sources.

The P_j/L_d histogram and dependence of P_j/L_d on λ_{Edd} for this sample of FR II quasars are plotted together with $z < 0.4$ FR II NLRGs in Fig. 1 and Fig. 2. As can be seen, the median jet production efficiency in FR II quasars is $\sim 0.02(\epsilon_d/0.1)$, i.e. ~ 13 times lower than in the $\lambda_{\text{Edd}} > 0.003$ subsample of $z < 0.4$ FR II NLRGs.

In Fig. 3 we show the P_j/L_d distributions for the FR II quasars divided into two subsamples, with $z > 1$ and $z < 1$. The fact that the P_j/L_d distributions are very similar for the high- and low-redshift subsamples indicates that the difference in median η_j between FR II quasars and $z < 0.4$ NLRGs at $\lambda_{\text{Edd}} > 0.01$ is not caused by cosmological evolution of jet production efficiency, but rather by the different flux limits and procedures to select the two samples.

Uncertainties of L_d luminosities derived in Shen et al. (2011) using bolometric corrections to optical luminosity at 5100 Å are about 0.1 dex (Richards et al. 2006), while uncer-

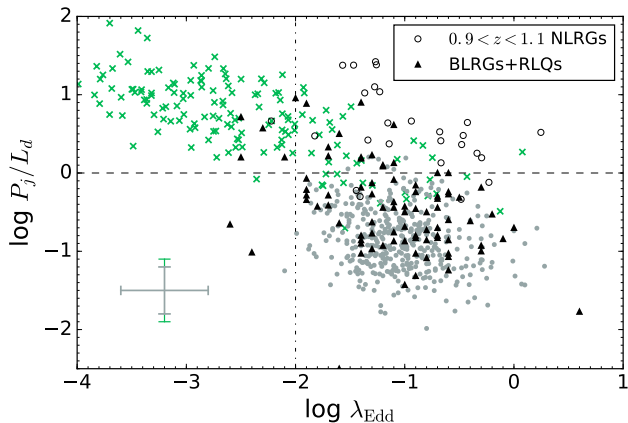


Figure 4. The same plot as in the Fig. 2 with two added samples: $0.9 < z < 1.1$ NLRGs as empty circles (27 sources); BLRG+RLQ as black triangles (87 sources). Uncertainties of P_j/L_d and λ_{Edd} for all four samples are presented in the lower left corner (their values for $z < 0.4$ FR II NLRGs and $0.9 < z < 1.1$ NLRGs and for FR II quasars and BLRG+RLQ are equal).

tainties of M_{BH} derived by Shen et al. using virial estimators are ~ 0.4 dex. With these uncertainties and 0.3 dex uncertainty of P_j , the uncertainties of P_j/L_d and λ_{Edd} for FR II quasars are ~ 0.3 dex and ~ 0.4 dex, respectively. They are marked, together with uncertainties for the $z < 0.4$ FR II NLRGs sample, in the lower left corner of Fig. 2.

2.4 $0.9 < z < 1.1$ sample of NLRGs

As we can see from Fig. 2, the sample of $z < 0.4$ FR II NLRGs is poorly represented at $\log \lambda_{\text{Edd}} > -1.5$. This is primarily due to a low number of high accretion rate AGNs with very massive BHs in the local Universe. In order to verify how much this incompleteness affects the average jet production efficiency in FR II RGs, we extend the FR II NLRGs sample by adding 27 $z \sim 1$ NLRGs selected in $0.9 < z < 1.1$ taken from Falder et al. (2010). With a few exceptions, they all have FR II radio morphologies. The relevant data for this sample are presented in the Table A3, which are taken from Table 1 in Fernandes et al. (2011), as well as Table 3 in Fernandes et al. (2015). As before, P_j is calculated based on Equation 2. The disc luminosity for this sample has been calculated using mid-IR data from *Spitzer Space Telescope* at wavelength $12 \mu\text{m}$ along with the following scaling relation: $L_d = 8.5 \times [\nu L_\nu]$ (Richards et al. 2006). Black hole masses have been derived using relation between the black hole and bulge masses (Håring & Rix 2004). Their uncertainty is ~ 0.3 dex. Combining it with uncertainty of disc luminosities, ~ 0.2 dex, and jet powers, 0.3 dex, gives uncertainties of P_j/L_d and of λ_{Edd} , both about 0.4 dex.

The sample is plotted in Fig. 4. The median P_j/L_d is similar to that of the $z < 0.4$ FR II NLRGs sample for $\lambda_{\text{Edd}} > 0.003$ and uncertainties of the $z \sim 1$ NLRGs sample are the same. They are marked in the lower left corner.

2.5 A BLRG+RLQ sample

The incompleteness of SDSS quasars at moderate accretion rates (Kelly & Shen 2013) may introduce a bias in our analysis of FR II quasars due to underrepresentation of such objects, particularly at $\lambda_{\text{Edd}} < 0.03$. In order to verify whether the incompleteness of SDSS quasars at moderate accretion rates can significantly affect the average value of η_j of our sample, we complete our studies of jet production efficiency by adding a sample of broad-line RGs co-selected with low redshift radio-loud quasars. The sample is comprised of radio-loud broad-line AGN with redshift $z < 0.4$, selected from Véron-Cetty & Véron (1989) by Eracleous & Halpern (1994, 2003) and used by Sikora et al. (2007) to study radio-loudness of these objects. Using a formal, luminosity related definition of quasars, these objects were divided by Sikora et al. into two subsamples: broad-line radio galaxies (BLRGs) and radio-loud quasars (RLQs). The BLRG+RLQ sample data are listed in Table A4a and A4b. As with the previous samples, P_j is calculated using Equation 2, but in this case, we have had to extrapolate flux densities at 5 GHz to 1.4 GHz using a radio spectral index $\alpha_r = 0.8$. The disc luminosity is calculated based on the B-band and using the bolometric correction from Richards et al. (2006). Its uncertainty is ~ 0.1 dex. Black hole masses have been derived using virial estimators (e.g. Woo & Urry 2002), and uncertainties of such estimators are ~ 0.4 dex. With these uncertainties and 0.3 dex uncertainty of P_j , the uncertainties of P_j/L_d and λ_{Edd} are ~ 0.3 dex and ~ 0.4 dex, respectively. They are marked in Fig. 4 in the lower left corner together with uncertainties for the $z \sim 1$ NLRGs sample. As we can see in Fig. 4, despite these large uncertainties, the BLRG+RLQ sample is fully consistent with the sample of FR II quasars from van Velzen et al.

3 DISCUSSION

The applicability of the MAD scenario for the production of powerful AGN jets was recently investigated using 3D general-relativistic, magnetohydrodynamic simulations (Igumenshchev 2008; Punsly et al. 2009; Tchekhovskoy et al. 2011; McKinney et al. 2012). These studies demonstrated that magnetically arrested discs have the ability to launch jets with a power comparable to the accretion power, as is required to explain the energetics of radio lobes in the radio-loudest FR II sources (Rawlings & Saunders 1991; Punsly 2007; Fernandes et al. 2011; Sikora et al. 2013).

However, the MAD simulations indicate there is a clear trend of decreasing efficiency of relativistic jet production with decreasing geometrical thickness of the accretion flow. This trend was found in the case of “non-radiative” models with disk thickness $H/R = 1.0 - 0.3$ (Tchekhovskoy et al. 2011; McKinney et al. 2012), and was explained as the being due to loading boundary layers of the Blandford-Znajek outflow with mass to such a level that these outflows do not gain relativistic speeds. More recently, simulations of the MAD scenario were extended by Avara et al. (2016) to cover the case of the optically thick accretion flows, with $H/R \sim 0.1$. Combining the results of these simulations with results obtained for non-radiative and geometrically thicker accretion flows they derived the following empirical formula

describing a dependence of the jet production efficiency η_j on geometrical thickness and dimensionless BH spin a ,

$$\eta_j \simeq 4a^2 \left(1 + \frac{0.3a}{1 + 2(H/R)^4} \right)^2 (H/R)^2, \quad (3)$$

which for $H/R \ll 1$ gives $\eta_j \sim 4a^2(1 + 0.3a)^2(H/R)^2$. According to the standard accretion disc model (Novikov & Thorne 1973; Laor & Netzer 1989), maximal thickness of a disc accreting onto a BH with $a \sim 1$ and producing radiation at a rate $\lambda_{\text{Edd}} \sim 0.1$ is $H/R \sim 0.04$. For these parameters the above formula gives $\eta_j \simeq 0.01$. This is a factor 2 less than the median value of the FR II quasars sample and by a factor 20 less than its upper bound in the P_j/L_d vs. λ_{Edd} plots. Noting ~ 0.4 dex uncertainties of P_j/L_d , it is rather unlikely that above discrepancy is resulting from errors of P_j and/or L_d . Then we can envisage two possible solutions of this discrepancy. One is that because MHD simulations of radiative, optically thick accretion flows are still not fully self-consistent, the extrapolation of dependence of η_j on H/R indicated by non-radiative accretion flows down to the regime of optically thick accretion flows can be quantitatively inaccurate. Another possibility is that optically thick accretion discs are much thicker than predicted by the standard accretion disc theory. The disc can be thicker in presence of strong toroidal magnetic fields (e.g. Begelman & Pringle 2007; Sądowski 2016), or can be accompanied by heavy, viscously driven corona (Różańska et al. 2015; Begelman et al. 2015). Furthermore, within the MAD zone the disc is radially balanced against gravity by dynamically dominated poloidal magnetic fields and, therefore, even if outside the MAD-zone the disc is geometrically thin, within the MAD-zone it can become sub-Keplerian and thicker than the standard one. The suspicion that approximations used by Avara et al. to treat in MHD simulations the optically thick disc are inaccurate is also supported by the fact, that they predict larger radiative efficiency of MADs than of standard accretion discs, whilst observations indicate the opposite: radio-quiet quasars have been found to be more luminous in UV than radio-loud quasars (Punsly et al. 2016, and refs. therein).

Obviously, not all radio-loud quasars have FR II radio morphology. According to de Vries et al. (2006), most of them have radio structures too compact to be resolved, or if resolved, are recorded as CSOs (Compact Symmetric Objects), CSS (Compact Steep-Spectrum) sources and GPS (GHz-peaked spectrum) sources (An & Baan 2012, and refs. therein). Many of them are as radio loud as FR II RGs and quasars and therefore can also be considered to involve MAD scenario. However, about 90 percent of all quasars are not detected in radio or have very weak radio emission which can be associated with starburst activities (Kimball et al. 2011) or with shocks formed by the quasar driven outflows (Zakamska & Greene 2014).

It is tempting to speculate, that the reason for a very small fraction of radio-loud quasars is associated with “a steep magnetic-flux function” of quasar precursors developed during a hot, quasi-spherical accretion phase, where the steepness can be determined by different levels of ordering in the magnetic fields that are advected to the center, and/or by the duration of the quasar pre-phase (Sikora & Begelman 2013). This scenario is schematically illustrated in Fig. 5. For a given amount of magnetic flux Φ_{tot} accumu-

lated during the quasar pre-phase (Bondi accretion phase), the MAD accretion mode will operate during a subsequent BLRG/quasar phase only if Φ_{tot} exceeds $\Phi_{\text{BH,max}}(\dot{M})$. One can easily deduce from this figure, that the fraction of objects operating in the MAD mode is predicted to increase with decreasing accretion rate. Such a trend is indicated at higher accretion rates by studies of quasars (Kratzer & Richards 2015), at moderate accretion rates – by studies of double-peak emission line galaxies (Wu & Liu 2004), and at very low accretion rates – by studies of nearby galaxies (Terashima & Wilson 2003; Chiaberge et al. 2005). Indications of a possible MAD scenario operation during the Bondi accretion phase have been recently provided by studies of $P_j/\dot{M}_{\text{Bondi}}$ in several nearby radio galaxies (Nemmen & Tchekhovskoy 2015).

Finally, we consider variability of the accretion rate as a possible complicating factor in our interpretation of the $P_j/L_d - \lambda_{\text{Edd}}$ distribution. The radio luminosity is related to the total energy content of the lobes, and is dependent on the time-averaged jet power averaged over the lifetime of the source. As a result, the jet power calculated from the lobe radio luminosity represents a measure of the time-averaged jet power. The hotspot luminosity may vary on short timescales due to variation in jet power, but the hotspots typically contribute only a small fraction of the total radio luminosity (Mullin et al. 2008), and so the integrated lobe luminosity will not be significantly affected by short timescale variation in the jet power. In contrast, the disc luminosity is a measure of instantaneous accretion rate, and the accretion rate may vary significantly on timescales much shorter than the lifetime of the radio galaxy. As a result, variability of the accretion disc luminosity will cause variability in the “apparent” jet production efficiency and Eddington ratio. Consider for example a source in which the accretion power varies by a factor of 10 between its maximum and minimum accretion rates. This object, if observed during its accretion rate minimum, will appear to have 10 times lower Eddington ratio and 10 times larger jet production efficiency than if it were observed at its accretion rate maximum. In effect, variability of the accretion rate will cause the $P_j/L_d - \lambda_{\text{Edd}}$ distribution to be stretched along a line with slope -1 in the $P_j/L_d - \lambda_{\text{Edd}}$ plane, broadly consistent with the slope of the distribution of points shown in Figure 4. Furthermore, for a duty cycle $\sim 1/2$, the object’s apparent jet production efficiency will be about 5 times larger than the true jet production efficiency when observed at its minimum accretion rate, and about 2 times smaller when observed at its maximum accretion rate. A natural driver of variability in the accretion rate is viscous instabilities in accretion discs (Janiuk et al. 2002; Janiuk & Czerny 2011). Observational support for this hypothesis may come from the spatial modulation of the radio brightness distributions seen in some large scale jets (Godfrey et al. 2012).

4 SUMMARY

The compilation of data on P_j/L_d and λ_{Edd} taken from four independently selected samples clearly show a drop of the jet production efficiency at higher accretion rates (Figure 4). It is tempting to connect this drop in jet production efficiency with a transition from radiatively inefficient, optically thin

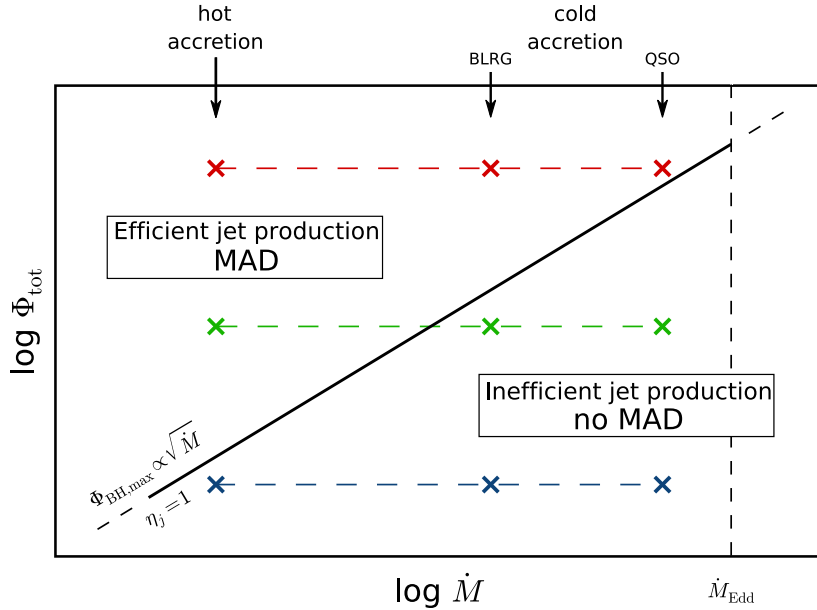


Figure 5. This figure illustrates a condition that must be satisfied in order to obtain a magnetically arrested disc, and also demonstrates how this condition dictates the fraction of radio loud AGN as a function of accretion rate, \dot{M} . The inner accretion flow will become magnetically arrested only if Φ_{tot} exceeds $\Phi_{\text{BH,max}}(\dot{M})$, where Φ_{tot} is the magnetic flux assumed to be accumulated in the central region of an AGN following the hot accretion phase preceding the higher accretion event associated with the BLRG or quasar phenomenon, while $\Phi_{\text{BH,max}}(\dot{M})$ is the maximal magnetic flux that can be confined on a BH by an accretion flow. For $\Phi_{\text{tot}} < \Phi_{\text{BH,max}}(\dot{M})$ the magnetic flux will be entirely enclosed on the black hole and the magnetically arrested disc will not be formed. It is assumed that efficient jet production (and therefore highly radio loud AGN) only occur in the MAD case, when $\Phi_{\text{tot}} > \Phi_{\text{BH,max}}(\dot{M})$, while jet production is assumed to be inefficient in the case of No MAD when $\Phi_{\text{tot}} < \Phi_{\text{BH,max}}(\dot{M})$. This condition implies that the fraction of AGN that are radio loud decreases with increasing \dot{M} . For details see [Sikora & Begelman \(2013\)](#).

accretion flows (RIAF) to the standard, optically thick accretion discs and assume that the key ingredient for jet production is the presence of the hot gas associated with the bulk accretion flow (at low accretion rates) or with the disc corona (at high accretion rates) (e.g. [Cao 2004](#); [Wu et al. 2013](#)). However, in order to produce at $\lambda_{\text{Edd}} > 0.01$ jets with P_j/L_d approaching unity, as is observed for many objects, requires magnetic fluxes in the central regions too large to be supported by disc coronas. This argument favors the MAD-scenario, but with a geometrical thickness of accretion flows much larger than the thickness predicted by standard theory. Whether the discs become thicker once entering the MAD-zone, or must be already thicker prior to the MAD-zone is the subject for future investigations.

ACKNOWLEDGEMENTS

We thank an anonymous referee for his/her critical comments which helped us to improve the paper. MS thanks Aleksander Sądowski for helpful discussions. The research leading to these results has received funding from the Polish National Science Centre grant 2013/09/B/ST9/00026 and from the European Research Council under the European Union’s Seventh Framework Programme (FP/2007-2013) / ERC Advanced Grant RADIOLIFE-320745.

REFERENCES

- An, T., & Baan, W. A. 2012, *ApJ*, 760, 77
 Antognini, J., Bird, J., & Martini, P. 2012, *ApJ*, 756, 116
 Avara, M. J., McKinney, J. C., & Reynolds, C. S. 2016, *MNRAS*, 462, 636
 Begelman, M. C., & Pringle, J. E. 2007, *MNRAS*, 375, 1070
 Begelman, M. C., Armitage, P. J., & Reynolds, C. S. 2015, *ApJ*, 809, 118
 Best, P. N., & Heckman, T. M. 2012, *MNRAS*, 421, 1569
 Bird, J., Martini, P., & Kaiser, C. 2008, *ApJ*, 676, 147
 Blandford, R. D., & Znajek, R. L. 1977, *MNRAS*, 179, 433
 Blundell, K. M., Rawlings, S., & Willott, C. J. 1999, *AJ*, 117, 677
 Blundell, K. M., & Rawlings, S. 2000, *AJ*, 119, 1111
 Cao, X. 2004, *ApJ*, 613, 716
 Chiaberge, M., Capetti, A., & Macchetto, F. D. 2005, *ApJ*, 625, 716
 de Vries, W. H., Becker, R. H., & White, R. L. 2006, *AJ*, 131, 666
 Elvis, M., Risaliti, G., & Zamorani, G. 2002, *ApJ*, 565, L75
 Eracleous, M., & Halpern, J. P. 1994, *ApJS*, 90, 1
 Eracleous, M., & Halpern, J. P. 2003, *ApJ*, 599, 886
 Falder, J. T., Stevens, J. A., Jarvis, M. J., et al. 2010, *MNRAS*, 405, 347
 Fanidakis, N., Baugh, C. M., Benson, A. J., et al. 2011, *MNRAS*, 410, 53
 Fernandes, C. A. C., Jarvis, M. J., Rawlings, S., et al. 2011, *MNRAS*, 411, 1909
 Fernandes, C. A. C., Jarvis, M. J., Martínez-Sansigre, A., et al. 2015, *MNRAS*, 447, 1184
 Garofalo, D., Evans, D. A., & Sambruna, R. M. 2010, *MNRAS*,

406, 975
 Godfrey, L. E. H., Lovell, J. E. J., Burke-Spolaor, S., et al. 2012, *ApJ*, 758, L27
 Godfrey, L. E. H., & Shabala, S. S. 2013, *ApJ*, 767, 12
 Häring, N., & Rix, H.-W. 2004, *ApJ*, 604, L89
 Igumenshchev, I. V. 2008, *ApJ*, 677, 317
 Janiuk, A., Czerny, B., & Siemiginowska, A. 2002, *ApJ*, 576, 908
 Janiuk, A., & Czerny, B. 2011, *MNRAS*, 414, 2186
 Kellermann, K. I., Sramek, R., Schmidt, M., Shaffer, D. B., & Green, R. 1989, *AJ*, 98, 1195
 Kelly, B. C., & Shen, Y. 2013, *ApJ*, 764, 45
 Kimball, A. E., Kellermann, K. I., Condon, J. J., Ivezić, Ž., & Perley, R. A. 2011, *ApJ*, 739, L29
 Körding, E. G., Jester, S., & Fender, R. 2006, *MNRAS*, 372, 1366
 Kratzer, R. M., & Richards, G. T. 2015, *AJ*, 149, 61
 Lacy, M., Ridgway, S. E., Sajina, A., et al. 2015, *ApJ*, 802, 102
 Laor, A., & Netzer, H. 1989, *MNRAS*, 238, 897
 Livio, M., Pringle, J. E., & King, A. R. 2003, *ApJ*, 593, 184
 Lu, Y., Wang, T., Zhou, H., & Wu, J. 2007, *AJ*, 133, 1615
 McKinney, J. C., Tchekhovskoy, A., & Blandford, R. D. 2012, *MNRAS*, 423, 3083
 Mingo, B., Hardcastle, M. J., Croston, J. H., et al. 2014, *MNRAS*, 440, 269
 Mullin, L. M., Riley, J. M., & Hardcastle, M. J. 2008, *MNRAS*, 390, 595
 Narayan, R., Igumenshchev, I. V., & Abramowicz, M. A. 2003, *PASJ*, 55, L69
 Nemmen, R. S., & Tchekhovskoy, A. 2015, *MNRAS*, 449, 316
 Netzer, H. 2009, *MNRAS*, 399, 1907
 Nipoti, C., Blundell, K.M., & Binney, J. 2005, *MNRAS*, 361, 633
 Novikov, I. D., & Thorne, K. S. 1973, *Black Holes (Les Astres Occlus)*, 343
 O’Dea, C. P., Daly, R. A., Kharb, P., Freeman, K. A., & Baum, S. A. 2009, *A&A*, 494, 471
 Punsly, B. 2007, *MNRAS*, 374, L10
 Punsly, B., Igumenshchev, I. V., & Hirose, S. 2009, *ApJ*, 704, 1065
 Punsly, B., Reynolds, C., Marziani, P., & O’Dea, C. P. 2016, *MNRAS*, 459, 4233
 Rafter, S. E., Crenshaw, D. M., & Wiita, P. J. 2011, *AJ*, 141, 85
 Rawlings, S., & Saunders, R. 1991, *Nature*, 349, 138
 Reynolds, C. S., & Begelman, M. C. 1997, *ApJ*, 487, L135
 Richards, G. T., Lacy, M., Storrie-Lombardi, L. J., et al. 2006, *ApJS*, 166, 470
 Różańska, A., Malzac, J., Belmont, R., Czerny, B., & Petrucci, P.-O. 2015, *A&A*, 580, A77
 Sądowski, A. 2016, *MNRAS*, 462, 960
 Shen, Y., Richards, G. T., Strauss, M. A., et al. 2011, *ApJS*, 194, 45
 Sikora, M., Stawarz, L., & Lasota, J.-P. 2007, *ApJ*, 658, 815
 Sikora, M., & Begelman, M. C. 2013, *ApJ*, 764, L24
 Sikora, M., Stasińska, G., Kozieł-Wierzbowska, D., Madejski, G. M., & Asari, N. V. 2013, *ApJ*, 765, 62
 Sołtan, A. 1982, *MNRAS*, 200, 115
 Tchekhovskoy, A., Narayan, R., & McKinney, J. C. 2011, *MNRAS*, 418, L79
 Terashima, Y., & Wilson, A. S. 2003, *ApJ*, 583, 145
 Tremaine, S., Gebhardt, K., Bender, R., et al. 2002, *ApJ*, 574, 740
 van Velzen, S., & Falcke, H. 2013, *A&A*, 557, L7
 van Velzen, S., Falcke, H., Körding, E. 2015, *MNRAS*, 446, 2985
 Véron-Cetty, M.-P., & Véron, P. 1989, *European Southern Observatory Scientific Report*, 7, 1
 Volonteri, M., Sikora, M., Lasota, J.-P., & Merloni, A. 2013, *ApJ*, 775, 94
 White, R. L., Helfand, D. J., Becker, R. H., Glikman, E., & de Vries, W. 2007, *ApJ*, 654, 99

White, S. V., Jarvis, M. J., Häußler, B., & Maddox, N. 2015, *MNRAS*, 448, 2665
 Willott, C. J., Rawlings, S., Blundell, K. M., & Lacy, M. 1999, *MNRAS*, 309, 1017
 Wilson, A. S., & Colbert, E. J. M. 1995, *ApJ*, 438, 62
 Woo, J.-H., & Urry, C. M. 2002, *ApJ*, 579, 530
 Wu, X.-B., & Liu, F. K. 2004, *ApJ*, 614, 91
 Wu, Q., Cao, X., Ho, L. C., & Wang, D.-X. 2013, *ApJ*, 770, 31
 Zakamska, N. L., & Greene, J. E. 2014, *MNRAS*, 442, 784

APPENDIX A: SAMPLES

Here we present astrophysical properties of our samples with detailed calculations described in Section 2. Complete tables are available as a supplementary material in the online journal. A portion is shown here for guidance regarding its form and content.

This paper has been typeset from a $\text{\TeX}/\text{\LaTeX}$ file prepared by the author.

Table A1. Radio and optical properties of $z < 0.4$ FR II NLRGs from Table 1 in [Sikora et al. \(2013\)](#) with some calculated values in this work. The disc luminosities L_d were determined using $L_{H\alpha}$.

SDSS ID	Cambridge Cat. ID	Redshift	$\log L_{1.4}$ [WHz $^{-1}$]	$\log L_{H\alpha}$ [L_{\odot}]	$\log L_{[O III]}$ [L_{\odot}]	$\log L_d$ [ergs $^{-1}$]	$\log P_j$ [ergs $^{-1}$]	$\log P_j/L_d$	$\log M_{BH}$ [M_{\odot}]	$\log \lambda_{Edd}$
0312.51689.471	4C +00.56	0.0524	25.34	7.605	7.572	44.497	44.4190	-0.0781	8.74	-2.3568
0349.51699.169	6C B165818.4+630042	0.1063	25.45	6.417	6.579	43.309	44.5133	1.2042	7.83	-2.6348
0366.52017.349	6C B171944.8+591634	0.2212	25.59	7.486	6.889	44.378	44.6333	0.2552	8.29	-2.0258
0432.51884.345	7C B073404.1+402639	0.3905	25.59	...	6.806	...	44.6333	...	8.66	...
0436.51883.010	6C B075738.1+435851	0.2554	25.66	6.899	6.740	43.791	44.6933	0.9022	8.42	-2.7428
0439.51877.637	7C B081405.1+450809	0.1422	25.43	5.690	6.322	42.582	44.4961	1.9140	8.17	-3.7018
0448.51900.335	6C B084421.9+571115	0.1937	26.08	7.515	7.887	44.407	45.0533	0.6462	7.98	-1.6868
0450.51908.330	4C +56.17	0.1409	26.05	7.107	6.912	43.999	45.0275	1.0284	8.04	-2.1548

Table A2. Some properties of FR II quasars from Table A1 in [van Velzen et al. \(2015\)](#). Few columns calculated in this work were added, together with black hole masses and Eddington ratios taken from [Shen et al. \(2011\)](#).

SDSS RA deg	SDSS Dec deg	Redshift	Lobe flux Jy	$\log L_{1.4}$ [WHz $^{-1}$]	$\log L_d$ [ergs $^{-1}$]	$\log P_j$ [ergs $^{-1}$]	$\log P_j/L_d$	$\log M_{BH}$ [M_{\odot}]	$\log \lambda_{Edd}$
2.910161	-10.749515	1.2712	0.0963	26.9061	46.5254	45.7613	-0.7641	9.65	-1.19
6.808142	1.610954	0.9010	0.1056	26.5880	45.6681	45.4887	-0.1794
10.165798	15.055892	0.8844	0.0294	26.0133	45.9686	44.9961	-0.9725
11.079023	-9.002630	0.9672	0.0509	26.3449	46.1815	45.2803	-0.9012	7.83	0.10
12.273874	-0.514230	3.2310	0.0196	27.1639	46.3095	45.9823	-0.3272
13.785633	-10.868412	1.3810	0.0303	26.4898	45.9742	45.4045	-0.5697
15.872669	0.681930	1.4331	0.1200	27.1259	46.6872	45.9497	-0.7375	9.47	-0.94
19.457974	-9.098518	0.8284	0.1041	26.4944	46.0661	45.4085	-0.6576	9.18	-1.34

Table A3. Properties from the Table 1 in [Fernandes et al. \(2011\)](#) and Table 3 in [Fernandes et al. \(2015\)](#) with added $\log P_j$ and $\log P_j/L_d$ values.

Cambridge Cat. ID	Redshift	$\log L_{\nu 151MHz}$ [WHz $^{-1}sr^{-1}$]	$\log L_d$ [ergs $^{-1}$]	$\log P_j$ [ergs $^{-1}$]	$\log P_j/L_d$	$\log M_{BH}$ [M_{\odot}]	$\log \lambda_{Edd}$
3C 280	0.997	28.29	46.7070	47.2258	0.5188	8.346	0.2467
3C 268.1	0.974	28.21	45.6890	47.1573	1.4683	7.476	0.0993
3C 356	1.079	28.12	46.4350	47.0801	0.6451	8.746	-0.4260
3C 184	0.994	28.01	45.6080	46.9858	1.3778	8.966	-1.4685
3C 175.1	0.920	27.98	45.5780	46.9601	1.3821	8.726	-1.2596
3C 22	0.937	27.96	46.8130	46.9430	0.1300	9.366	-0.6676
3C 289	0.967	27.95	46.2710	46.9344	0.6634	9.096	-0.9393
3C 343	0.988	27.78	46.5940	46.7887	0.1947	8.776	-0.2958

Table A4a. Some properties of BLRGs from Table 1 in [Sikora et al. \(2007\)](#) with calculated properties in this work.

IAU	Name	Redshift	m_V	A_V	κ_*	$\log L_B$ [ergs $^{-1}$]	F_5 Jy	$\log L_R$ [ergs $^{-1}$]	$\log P_j$ [ergs $^{-1}$]	$\log P_j/L_d$	$\log M_{\text{BH}}$ [M_\odot]	$\log \lambda_{\text{Edd}}$
0038-0207	3C 17	0.220	18.0	0.08	0.58	43.9	2.48000	43.2	45.7920	0.8920	8.7	-1.9
0044+1211	4C +11.06	0.226	19.0	0.26	0.28	43.8	0.22000	42.2	44.9349	0.1349	7.8	-1.1
0207+2931	3C 59	0.110	16.0	0.21	0.28	44.4	0.67000	42.0	44.7634	-0.6366	8.9	-1.6
0224+2750	3C 67	0.311	18.6	0.42	0.82	43.8	0.87000	43.1	45.7063	0.9063	8.1	-1.4
0238-3048	IRAS 02366-3101	0.062	15.0	0.22	0.30	44.2	0.00343	39.2	42.3634	-2.8366	8.6	-1.5
0238+0233	PKS 0236+02	0.207	17.7	0.11	0.46	44.1	0.12000	41.9	44.6777	-0.4223	8.8	-1.8
0312+3916	B2 0309+39	0.161	18.2	0.49	0.10	44.0	0.82200	42.5	45.1920	0.1920	8.3	-1.4
0342-3703	PKS 0340-37	0.285	18.6	0.03	0.19	44.2	0.71000	42.9	45.5349	0.3349	8.8	-1.7

Table A4b. The content of the table is analogous to the Table [A4a](#), but for RLQs instead of BLRGs.

IAU	Name	Redshift	m_V	A_V	κ_*	$\log L_B$ [ergs $^{-1}$]	F_5 Jy	$\log L_R$ [ergs $^{-1}$]	$\log P_j$ [ergs $^{-1}$]	$\log P_j/L_d$	$\log M_{\text{BH}}$ [M_\odot]	$\log \lambda_{\text{Edd}}$
0019+2602	4C 25.01	0.284	15.4	0.10	0.00	45.6	0.405	42.7	45.3634	-1.2366	9.1	-0.6
0113+2958	B2 0110+29	0.363	17.0	0.21	0.00	45.2	0.311	42.8	45.4491	-0.7509	9.2	-1.1
0157+3154	4C 31.06	0.373	18.0	0.18	0.11	44.8	0.394	43.0	45.6206	-0.1794	9.1	-1.4
0202-7620	PKS 0202-76	0.389	16.9	0.17	0.00	45.3	0.800	43.3	45.8777	-0.4223	9.2	-1.0
0217+1104	PKS 0214+10	0.408	17.0	0.36	0.01	45.4	0.460	43.1	45.7063	-0.6937	8.9	-0.7
0311-7651	PKS 0312-77	0.225	16.1	0.32	0.00	45.2	0.590	42.6	45.2777	-0.9223	8.4	-0.3
0418+3801	3C 111	0.049	18.0	5.46	0.04	45.1	6.637	42.3	45.0206	-1.0794	8.8	-0.8
0559-5026	PKS 0558-504	0.138	15.0	0.15	0.00	45.1	0.121	41.5	44.3349	-1.7651	7.4	0.6